Faculty of Electrical Engineering
Universiti Teknologi Malaysia

VOL. 13, NO. 2, 2011, 12-20

ELEKTRIKA
http://conf.fke.utm.my/elektrika

# Analysis and Verification of the Effects of Active Damping on the Dynamic Performance of a Grid-Side Converter

**Cajethan Abuchi Nwosu**[1], and **Cosmas Uchenna Ogbuka**[1]

[1] Department of Electrical Engineering, University of Nigeria, Nsukka, Nigeria.

**Abstract:** One of the most important aspects for large scale integration of wind power systems is the fault ride through (FRT) capability with frequency and voltage stabilization. Large voltage sags induce high voltages in the rotor circuit of the DFIG and thus the rotor current rises and could exceed the current capability of the converter switches. Dynamic performances of a grid-side converter (GSC) to grid voltage sags and fault conditions with active damping and without active damping are presented. Under the same control platform, a faster dynamic response is achieved for the DC-link voltage when active damping is considered as against a sluggish and ripple-infested response without active damping. Under fault condition, a 42% decrease in DC-link voltage is realized when active damping is considered. This is against 136% increase in the DC-link voltage that may excite the protective system to disconnect the grid-side converter subsystem from the rest of the network and thus disenable the ride-through capability of the GSC subsystem when active damping is not considered.

**Keywords:** Grid-side converter, active damping, dynamic response, internal model control (IMC).

## 1. INTRODUCTION

Power electronic back-to-back converter is the optimum choice for the control of rotor current of a doubly-fed induction generator in order to vary the slip power for variable speed constant frequency operation [1, 2, 3]. The back-to-back converter comprises two PWM converters with a common DC bus which makes the system flexible for the control of active and reactive power flow. Wind turbines often do not take part in voltage and frequency control and if a disturbance occurs, the wind turbines are disconnected and reconnected when normal operation has been restored [3]. New grid codes are however emerging to ensure that wind turbines would contribute to the control of voltage and frequency and also to stay connected to the grid network following a disturbance [2, 4]. What this means is that wind turbines should be able to continuously supply the network during sudden jumps in grid voltages.

To be able to maintain a ride through capability of wind turbines connected to the network in the events of voltage sags and fault occurrences, efficient control methodology is required for the back-to-back converter feeding the rotor circuit. A properly designed control scheme can smooth out the time-varying load that may be transmitted through the converter to the generator components. In the paper, we limit the cope of study to the verification of the effects of active damping on the dynamic performance of grid-side converter in the events of sudden changes in the grid voltages. In this verification, we assume that the converter is ideal and that the DC-link will always remain constant. This means that the converter must have to be shielded from disturbances external and internal to it; or that the disturbances even when they affect the DC-link voltage, are damped out in good time in order not to excite the protective breaker.

Standard vector control technique usually adopted for the control of grid-side converter comprises the outer loop DC-link voltage control and inner loop current control which together aim at achieving constant DC-link voltage control which together aim at achieving constant DC-link voltage. The active damping proposed here is for both the outer voltage control and inner current control. In addition to contributing to stabilizing and damping the converter response to any command input, the major function of the active damping in the voltage control is to compensate for the added factor in the design of the voltage controller. The bulk of stabilizing and damping of the grid-side converter control is carried out by the active damping in the inner current control loop.

The aim of active damping is to design controllers that emulate resistive output impedance for the converters by introducing additional control loops for the power electronic converters controls. The 'emulated resistance' will increase the damping of the grid, making it less sensitive to harmonics and oscillations. Usually the dynamics of a process (the open loop transfer function) is much slower than the dynamics of the closed-loop system; any disturbance rejection is to a large extent determined by the process. Therefore, addition of an inner feed-back loop, see Figs. 2b and 3, can improve the disturbance rejection.

## 2. THE MODEL OF LINE INDUCTANCE

Let us first develop the model of three-phase line inductances which are linked to the rotor circuit of a doubly-fed induction machine through a back-to-back converter. Here, we consider only the grid-side converter control which has the capacity to: maintain the DC-link voltage in a set value; maintain the balance between the DC-link power and power supplied to the grid and; guarantee a converter operation with unity power factor [4, 5]. The voltage balance across the filter inductors in Fig. 1 is:

$$v_a = Ri_a + L\frac{di_a}{dt} + v_{a1}$$
$$v_b = Ri_b + L\frac{di_b}{dt} + v_{b1} \quad (1)$$
$$v_c = Ri_c + L\frac{di_c}{dt} + v_{c1}$$

where $v_a$, $v_b$, and $v_c$ are the three phase grid voltages, $v_{a1}$, $v_{b1}$, and $v_{c1}$ are the front-end converter voltages, and $i_a$, $i_b$, and $i_c$ are the line currents. L and R are the filter inductance and resistance. Applying phase and rotation transformations to Eq. (1), the governing equations of the current loop dynamics in the two axes can be written as follows:

$$L\frac{di_d}{dt} + Ri_d - \omega_e Li_q + v_{d1} = v_d \quad (2)$$
$$L\frac{di_q}{dt} + Ri_q + \omega_e Li_d + v_{q1} = v_q \quad (3)$$

$v_d$ and $v_q$, $i_d$ and $i_q$, and $v_{d1}$ and $v_{q1}$ are the d- and q-axis components of the gird voltages, line currents, and front-end converter voltages respectively. The terms $\omega_e L_i d$ and $\omega_e Li_q$ are known as rotational emfs which appear as cross-coupling terms due to the transformations. In this model, we align the d-axis of the reference frame along the grid-voltage position so that $v_q = 0$.

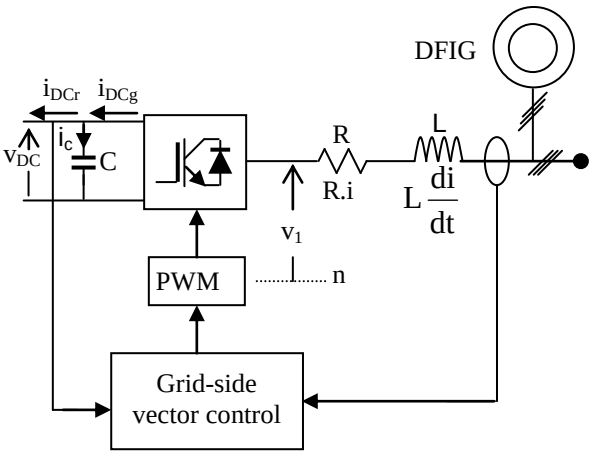


**Fig. 1** Grid-side converter arrangement.

The d-q axis components of the converter reference voltages (or terminal voltage vectors of front-end converter) may be written as:

$$v_{d1}^* = -Ri_d - L\frac{di_d}{dt} + (\omega_e Li_q + v_{d1}) \quad (4)$$
$$v_{q1}^* = -Ri_q - L\frac{di_q}{dt} - (\omega_e Li_d) \quad (5)$$

where the terms in the brackets constitute the decoupling terms.

In the conventional control of the grid-side converter, the rotational emfs which appear as cross-coupling terms due to the transformations are compensated to produce proper decoupling between the axes. The influence of the rotational emfs which also appear as cross-coupling terms in the control of rotor-side converter is regarded as minor (relative to the back emf which also exists) [6] that can be catered for by the Pl controller in each axis. Owing to the absence of back emf in Eqs. (4) and (5), the influence of the rotational emfs becomes prominent that only their compensation does not guarantee for fast dynamic response of the system. In order to enhance the stability of the grid-side converter control and improve its dynamic response an active damping is introduced in each of the inner current control loops in addition to the compensation. Active damping is also included in the outer voltage control loop to offset the added factor of correction in the voltage controller whose plant has hitherto one pole at the origin prior to the application of internal model control (IMC). The inclusion of active damping also compensates for the disturbance due to the rotor-side DC-link current $i_{DCr}$.

## 3.0 CONTROLLER STRUCTURE SET-UPS

### 3.1 Inner Loop Current Controller

Just before the addition of the active damping, the plant for the grid-side converter is derived from the transfer function from $v_{dq}$ as input to $i_{dq}$ as output as:

$$G(s) = \frac{i_d(s)}{v_d(s)} = \frac{i_q(s)}{v_q(s)} = \frac{1}{sL + R} \quad (6)$$

The grid-side converter is modeled as:

$$k_{c1} = \frac{m_1 E}{2V_{tri}} \quad (7)$$

where E is the DC-link voltage, $m_1$ is the grid-side converter modulation index, and $V_{tri}$ is the amplitude of the triangular carrier signal. Through the application of IMC [4] the controllers are obtained as:

$$C(s) = \frac{\alpha_{dq} L}{k_{c1}} + \frac{\alpha_{dq} R}{sk_{c1}} \quad (8)$$

with gains:

$$k_{pdq} = \frac{\alpha_{dq} L}{k_{c1}}; \quad k_{idq} = \frac{\alpha_{dq} R}{k_{c1}} \quad (9)$$

The d-axis and q-axis current control laws are:

$$v_d^* = -v_d' + (\omega_e Li_q + v_d)$$
$$v_q^* = -v_q' - (\omega_e Li_d) \quad (10)$$

where $v_d^*$ and $v_q^*$ are the reference values for the GSC, $v_d'$ and $v_q'$ are the uncompensated voltages which in this case are the same as outputs of the d- and q-axis PI controllers given by:

$$v'_d = \left(k_{pd} + \frac{k_{id}}{s}\right)\left(i_d^{ref} - i_d\right)$$

$$v'_q = \left(k_{pq} + \frac{k_{iq}}{s}\right)\left(i_q^{ref} - i_q\right) \quad (11)$$

The terms in brackets constitute voltage-compensation terms, and $v_d$ is the d-axis transformed voltage.

By the introduction of active damping, the uncompensated voltages change to:

$$v'_d = v''_d - R_a i_d$$

$$v'_q = v''_q - R_a i_q \quad (12)$$

where $R_a$ is known as active resistance or active damping. By this introduction, the d-axis and q-axis current control laws change to:

$$v_d^* = -(v''_d - R_a i_d) + (\omega_e L i_q + v_d)$$

$$v_q^* = -(v''_q - R_a i_q) - (\omega_e L i_d) \quad (13)$$

where $v''_d$ and $v''_q$ are now the outputs of the d- and q-axis PI controllers but different from the uncompensated voltages. To this end, the inner closed-loop transfer function, assuming ideal parameters, becomes:

$$G_{dq}(s) = \frac{i_{dq}(s)}{v'_{dq}(s)} = \frac{1}{sL + R + R_a} \quad (14)$$

Then, by utilizing IMC and taking into consideration the converter model, the following PI controller for the d and q frames is obtained:

$$C(s) = \frac{\alpha}{s}(k_{c1}G_{dq})^{-1}(s) = \frac{\alpha L}{k_{c1}} + \frac{\alpha(R + R_a)}{sk_{c1}} \quad (15)$$

where α is the closed-loop bandwidth of the inner current control. The active damping may be chosen as $R_a = \alpha_{dq}L - R$ [8] for effective damping of the inner-loop current control. The dq-axis current control law can be written as:

$$v_d = \left(k_{pd} + \frac{k_{id}}{s}\right)\left(i_d^{ref} - i_d\right) - R_a i_d$$

$$v_q = \left(k_{pq} + \frac{k_{iq}}{s}\right)\left(i_q^{ref} - i_q\right) - R_a i_q \quad (16)$$

The gains are:

$$k_{pdq} = \frac{\alpha_{dq}L}{k_{c1}},\ k_{idq} = \frac{\alpha_{dq}(R + R_a)}{k_{c1}} \quad (17)$$

Fig. 2a is the structure of the conventional grid-side current-control for the d-q axis loops. Fig. 2b is the resulting structure when the active resistance $R_a$ is added.

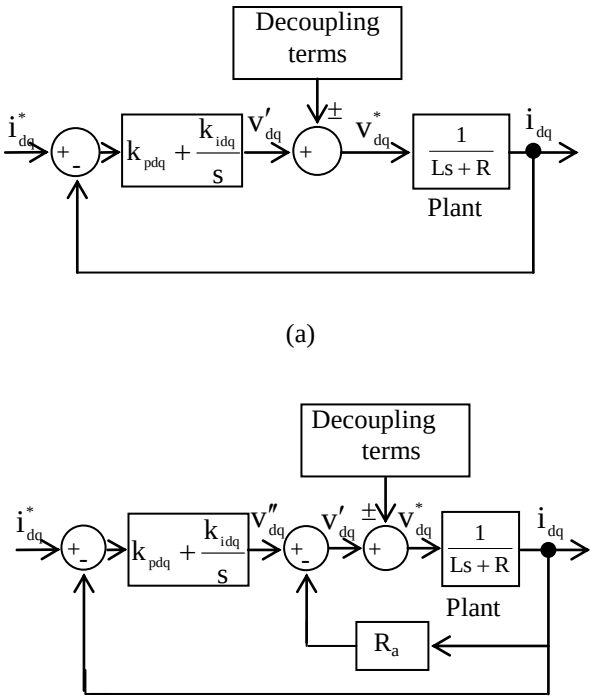


**Fig. 2** Grid-side current control loop: (a) conventional structure (b) structure with active resistance.

### 3.2 Outer Loop DC-link Voltage Controller

Fig. 3 shows the DC-link voltage control loop where $G_a$ is known as active conductance, performing the active damping. The power balance between the DC-link and the grid-side converter output gives [9, 10]:

$$v_{DC}i_{DCg} = 3v_d i_d \quad (18)$$

with the following relationships:

$$v_d = \frac{m_1}{2\sqrt{2}}v_{DC} \quad (19)$$

$$i_{DCg} = \frac{3}{2\sqrt{2}}m_1 i_d \quad (20)$$

The plant for the DC-link voltage control is derived from the transfer function of the dynamics of the DC-link as:

$$G(s) = \frac{v_{DC}(s)}{i_d(s)} = k\frac{1}{sC} \quad (21)$$

where $k = \frac{3}{2\sqrt{2}}m_1$ is the grid-side converter constant for the voltage controller. It is observed that the resulting

transfer function has a pole at the origin and thus pose some level of difficulty controlling it. One solution is to add an inner feedback loop for active damping as [11]:

$$i_d = i_d^{'} - G_a v_{DC} \tag{22}$$

where $i_d^{'}$ is the reference current provided by the outer control loop. The plant is then remodeled as:

$$G'(s) = \frac{v_{DC}(s)}{i_d^{'}(s)} = \frac{k}{sC + kG_a} \tag{23}$$

And by the application of IMC principle, the Pl controller is obtained as:

$$C(s) = \frac{\alpha C}{k} + \frac{\alpha G_a}{s} \tag{24}$$

with gains:

$$k_p = \frac{\alpha C}{k}, \quad k_i = \alpha G_a \tag{25}$$

where α is the closed-loop bandwidth of the outer voltage control (different from that for the inner current control). In order that the disturbance due to the rotor-side converter current $i_{DCr}$, be damped with the same bandwidth as the DC-link voltage control loop, we let $G_a = \alpha C$.

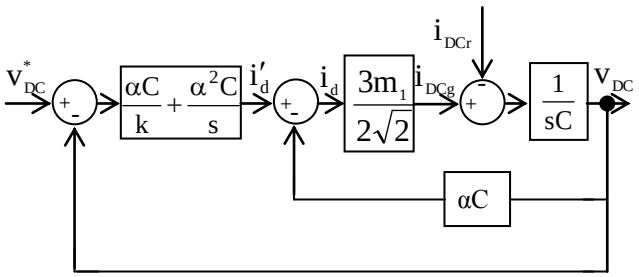


**Fig. 3** DC-link voltage control.

The complete control structure for the grid-side converter is shown in Fig. 4. The direct axis current component of the converter is actively controlled in order to regulate the DC-link voltage $v_{DC}$ and maintain the balance between the DC-link power and power supplied to the grid. The damping factors, $G_a$ and $R_a$ shown in dotted lines in Fig. 4, have been appropriately selected.

It is recommended that the closed-loop bandwidth be related to the angular sampling frequency and angular switching frequency as [12]:

$$\omega s \geq 10\alpha, \text{ and } \omega_{sw} \geq 5\alpha \tag{26}$$

A switching frequency of 1950Hz, which gives frequency modulation ratio of 39, is chosen for the grid-side converter. This gives an approximate angular switching frequency of 12252rad/s. By Eqn. (26), closed-loop bandwidth and sampling time of 2250rad/s and 0.1ms were selected for the inner current control while closed-loop bandwidth and sampling time of 225rad/s and 1ms were selected for the outer voltage control respectively.

The 3-phase currents and voltages are first transformed into a two axis α,β stationary frame (Clarke transform), and then into another 2-axis dq reference frame rotating at the grid frequency (Park transform). The angular position of the supply voltage vector is calculated as:

$$\theta_e = \int \omega_e dt = \tan^{-1} \frac{v_\beta}{v_\alpha} \tag{27}$$

where $v_\alpha$ and $v_\beta$ are the α, β (stationary 2-axis) stator voltage components. By aligning the d-axis of the reference frame along the stator (grid) voltage position, $v_q$ is zero and thus the active and reactive power flow is calculated as follows:

$$P = \frac{3}{2} v_d i_d \tag{28}$$

$$Q = \frac{3}{2} v_d i_q \tag{29}$$

## 4. SIMULATION RESULTS

A number of simulations are carried out to study the performance of the grid-side converter in both transient and steady-state conditions; when active damping is included in the inner current control loops and when it is not included. The Matlab/Simulink software model is utilized in this study. The primary aim is to regulate the DC-link voltage at 550V. This sets the line-to-line AC voltage approximately to 250V for a modulation factor of 0.75. The d-axis current demand is derived from the DC-link outer voltage control loop, while the q-axis current demand is set at zero. The parameters used in the simulations are as listed in table 1 while the complete control structure for the grid-side converter is shown in Fig. 4.

**Table 1:** Parameters used in the simulations.

| | |
|---|---|
| Filter inductance (L) | 12mH |
| Filter resistance (R) | 0.1Ω |
| DC-link capacitor (C) | 2.4mF |
| Grid frequency ($f_e$) | 50Hz |
| Grid-side converter modulation depth ($m_1$) | 0.75 |

### 4.1 Normal operating condition

Under normal operating condition, Fig. 5 shows the comparison of DC-link voltages with active damping and without active damping. The DC-link voltage attains the steady-state value of about 550V shortly after about 0.35s when active damping is included. In the absence of active damping, the DC-link voltage attains about same steady-state value after about 1.6s. Fig. 6 and Fig. 7 show the DC-link currents without and with active damping respectively. Fig. 8 shows phase 'A' modulation (reference) voltage when active damping is not considered, while Fig. 9 is its representation when active damping is considered.

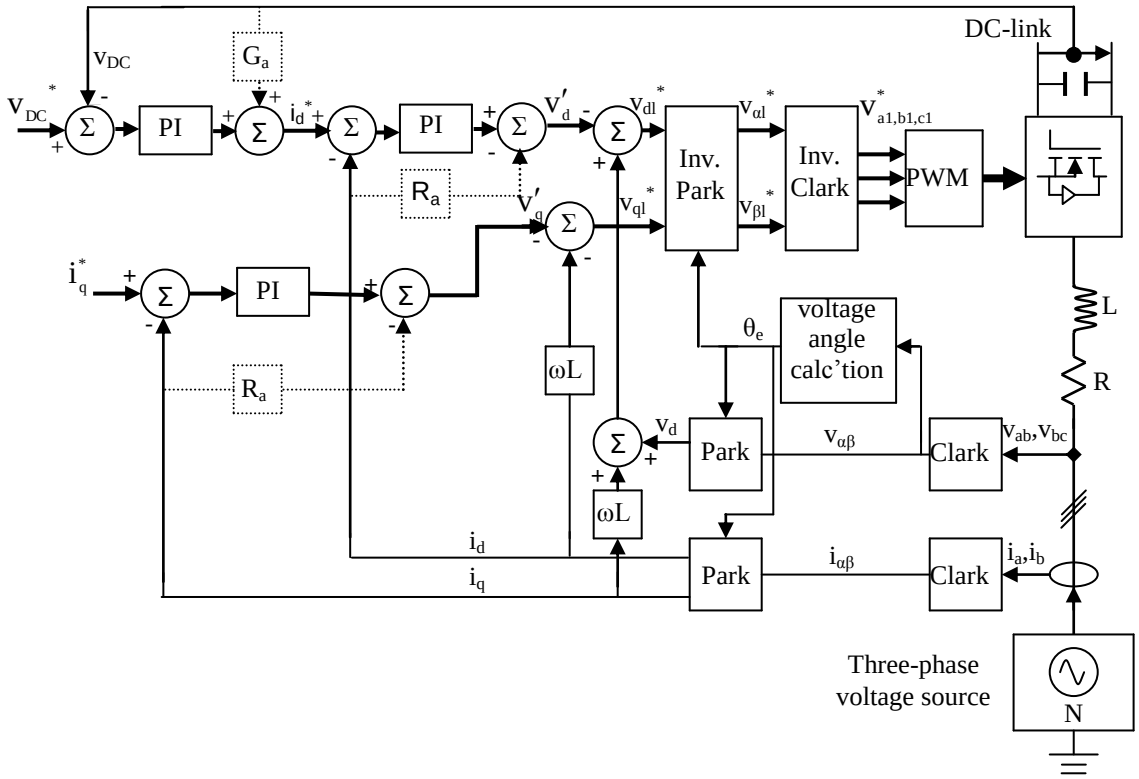


**Fig. 4** The complete control structure for the grid-side converter.

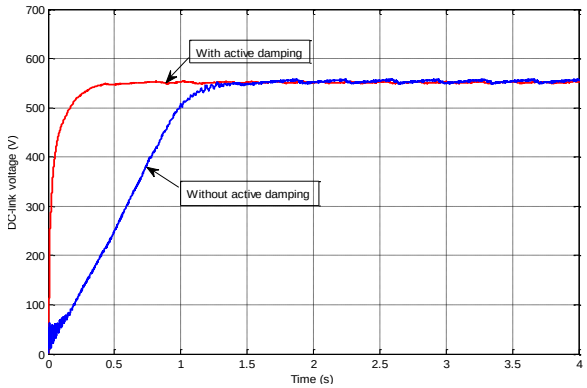


**Fig. 5** DC-link voltages.

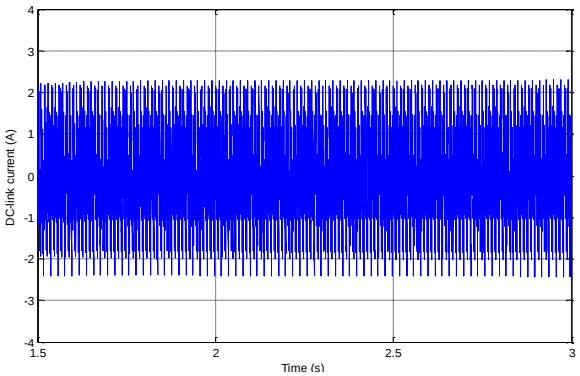


**Fig. 7** DC-link current with active damping.

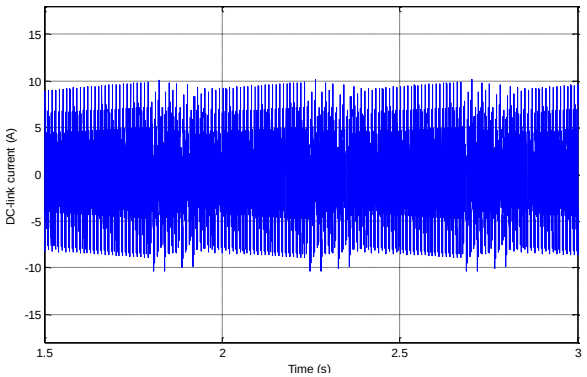


**Fig. 6** DC-link current without active damping.

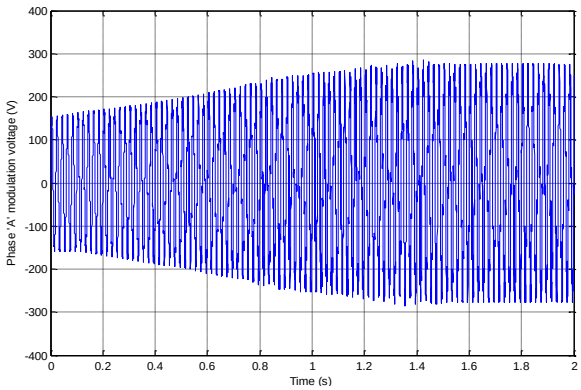


**Fig. 8** Phase 'A' modulation voltage.

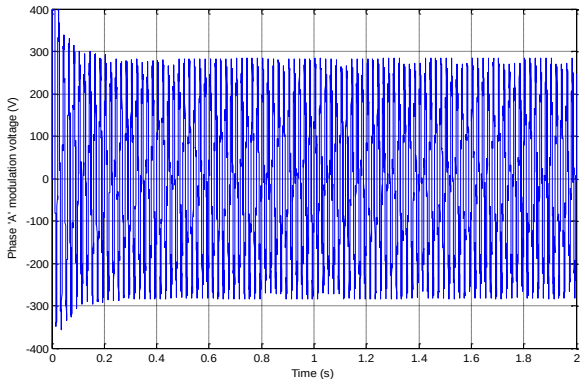


**Fig. 9** Phase 'A' modulation voltage.

### 4.2 Voltage sag profile

In order to investigate the dynamic response of the grid-side converter to grid voltage sag, a 50 per cent grid voltage dip was simulated from a three-phase Simulink voltage block. The dip was applied at t = 2s and lasts for 0.5s. The grid in turn comprises an 11kV source connected to a three-phase three winding transformer. One output of the transformer feeds a stepped down 250V to the GSC, while the second output supplies a stepped down 400V to the stator of the DFIG. Fig. 10 shows the phase-to-phase stator voltage with a 50 per cent dip. Fig. 11 shows the comparison of DC-link voltages with active damping and without active damping. With active damping, the DC-link voltage decreases exponentially to about 517.5V. After the removal of the dip, it starts to increase exponentially and after about 0.2s it once again attained the steady state. Without active damping, the DC-link voltage increases exponentially to a maximum value of about 580V and then decays to the 550V steady state value 0.3s later. Fig. 11 shows the comparison of dynamics of the DC-link currents in responses to 50% grid voltage dips. Fig. 12 and Fig. 13 are the DC-link currents without and with active damping respectively. Fig. 14 and Fig. 15 are the resulting modulation voltages without active damping and with active damping respectively. In the two Figures, the 50% grid voltage dip is manifested in the sinusoidal reference voltages.

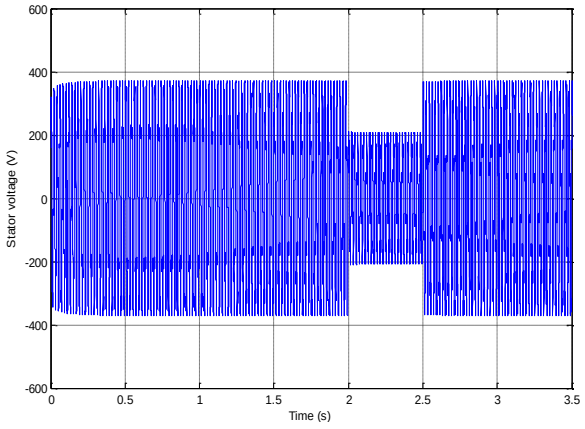


**Fig. 10** Phase-to-phase stator voltage with a 50 per cent dip.

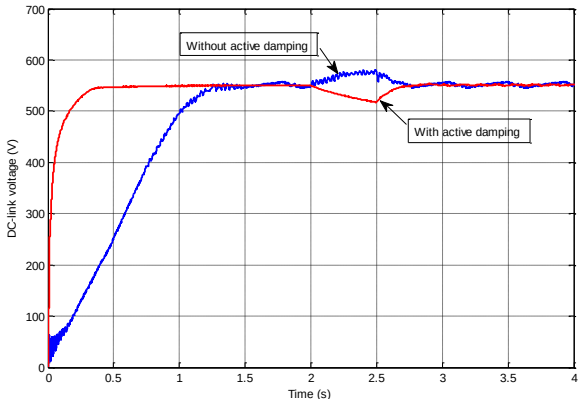


**Fig. 11** DC-link voltages.

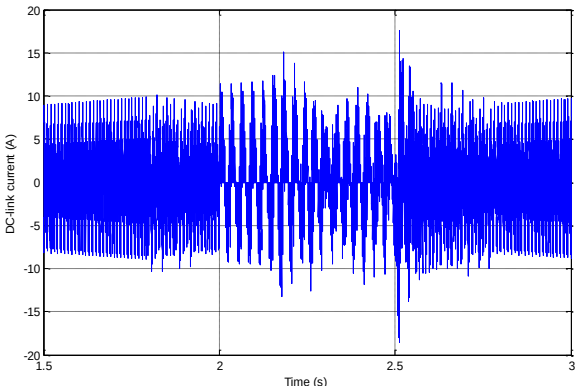


**Fig. 12** DC-link current without active damping.

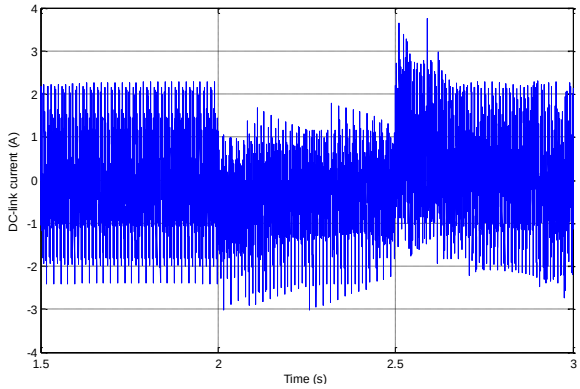


**Fig. 13** DC-link current with active damping.

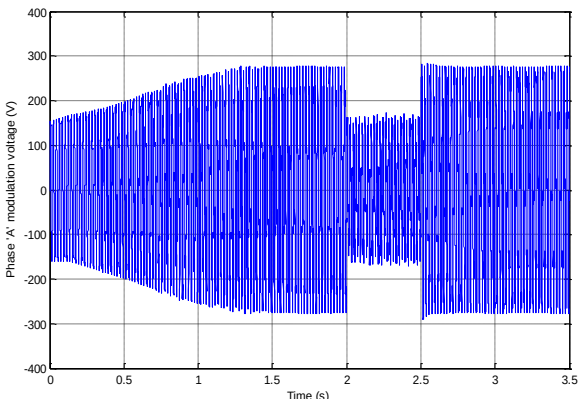


**Fig. 14** Phase 'A' modulation voltage.

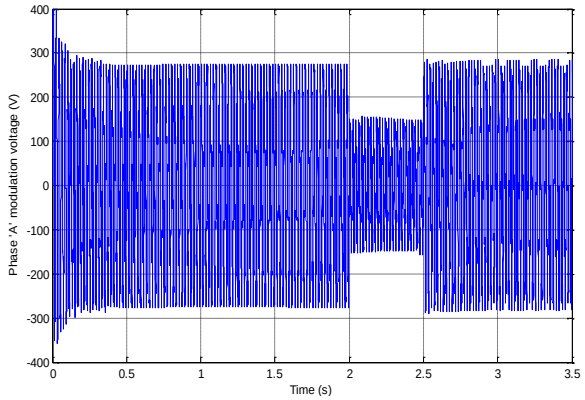


**Fig. 15** Phase 'A' modulation voltage.

### 4.3 Fault conditions

For the investigations of the dynamic response of the GSC under fault conditions, the same grid condition as simulated above is used. In addition, however, the effect of the X/R ratio i.e. the short-circuit impedance given by tan $\varphi_{sc} = X_{sc}/R_{sc}$ is taken into account in the grid. A three-phase short-circuit level of 10MVA with two X/R ratio of 3 and 10 is considered. A three-phase to ground fault with a fault resistance of 0.1Ω is applied to the network at t = 2s for 0.5s. As can be seen in Fig. 16, the dip in the stator voltage is about 77.3%. Fig. 17 is the resulting DC-link voltages at X/R ratio of 3. At the application of the fault when active damping is considered, the DC-link voltage decreases and oscillates temporarily between about 240V and 492V and after about 0.1s settles at about 400V. It then starts to decrease exponentially to 320V. At the clearing of the fault, the voltage rises almost instantly to about 470V before it starts to increase exponentially and after about 0.25s attains the steady state value of 550V.

At the application of fault with active damping removed, the DC-link voltage rises exponentially and at a faster rate from about 550V to about 1300V. At the clearing of the fault, it decreases also exponentially but in an oscillatory manner to about 370V 0.3s latter. It then starts to increase and after about 0.6s it attains and maintains another near-steady state value of 650V, about 100V greater than the initial steady state value. Fig. 18 and fig. 19 show the variations of the DC-link currents under fault conditions without active damping and with active damping respectively. Fig. 20 and Fig. 21 are the resulting modulation voltages without active damping and with active damping respectively.

The effects of the short-circuit impedance on the dynamics of the GSC in relation to the DC-link voltage is investigated. For the two values of X/R ratios, Fig. 22 represents the simulation results for for non-active damping conditions. With active damping, the variations of the DC-link voltage for the two cases of X/R ratios appear the same under same fault conditions.

Without active damping, the responses of the DC-link voltage to same fault conditions with the two X/R ratios appear the same before the fault and just before the removal of the fault. Their responses start to vary at the removal of the fault and may never attain the same steady state again. For the X/R ratio = 3, the DC-link voltage remains at the new value of about 650V, while for X/R = 10, the DC-link voltage finally assumes its initial steady state of 550V about 1.25s after the removal of the fault.

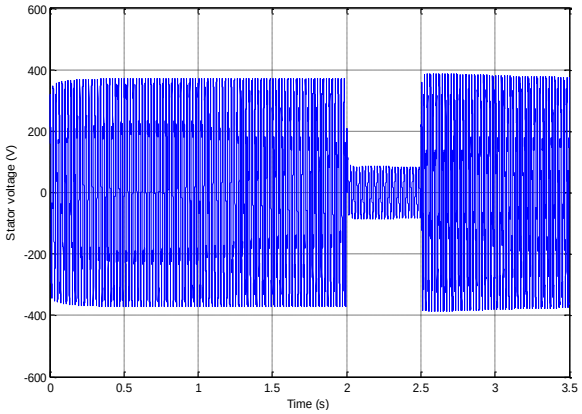


**Fig. 16** Phase-to-phase stator voltage.

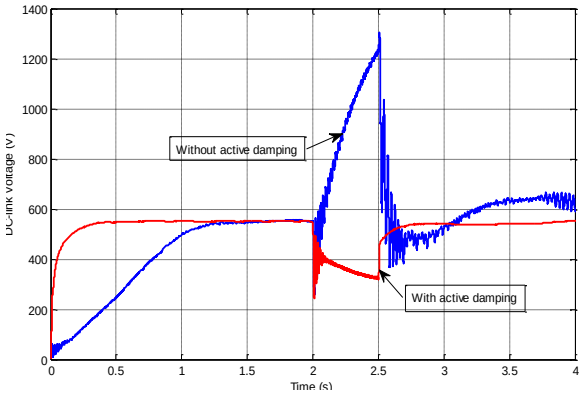


**Fig. 17** DC-link voltages.

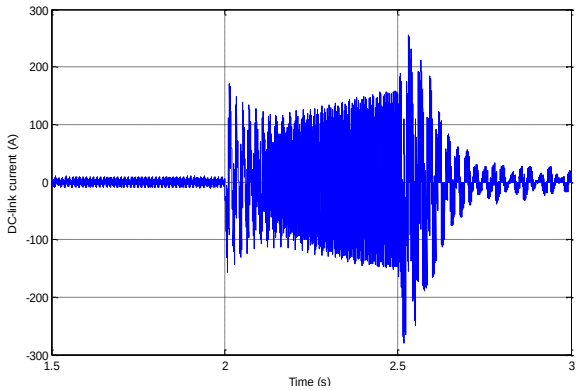


**Fig. 18** DC-link current without active damping.

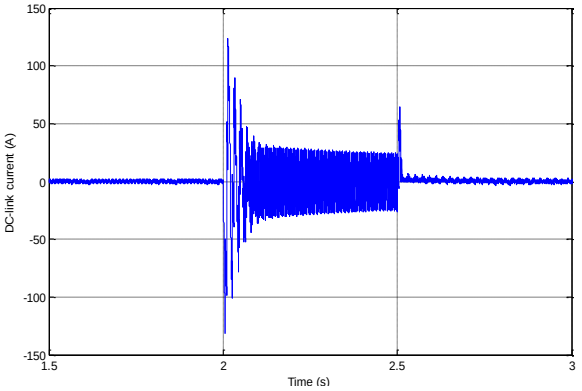


**Fig. 19** DC-link current with active damping.

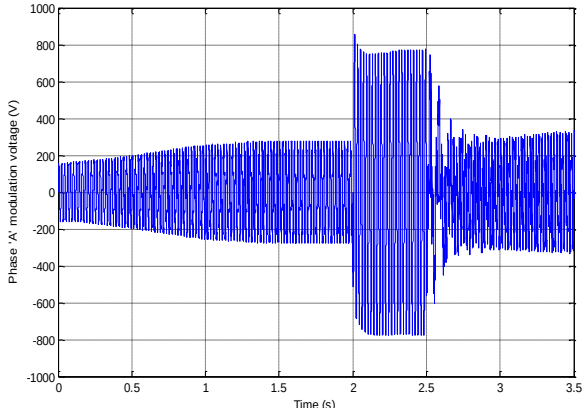


**Fig. 20** Phase 'A' modulation voltage.

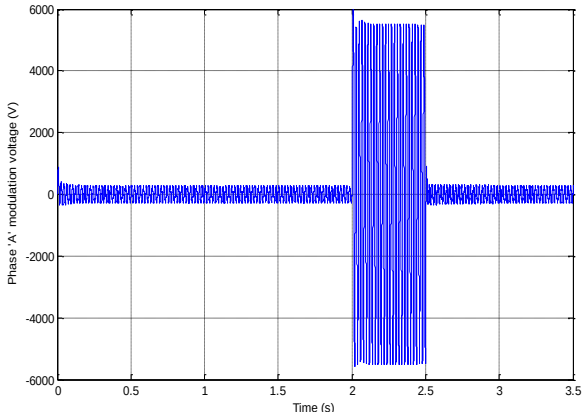


**Fig. 21** Phase 'A' modulation voltage.

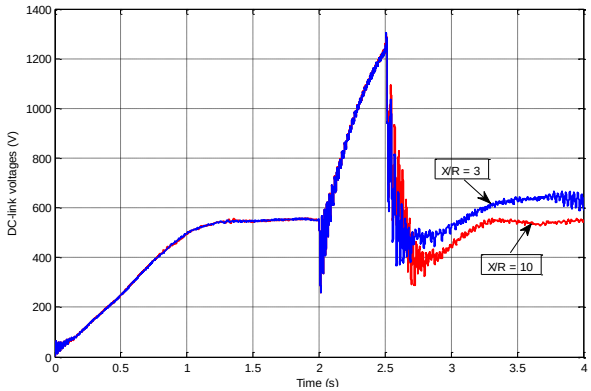


**Fig. 22** DC-link voltages for X/R = 3, and 10.

### 4.4 Discussion of results

Under normal operating conditions, it is observed that the DC-link voltage attains the steady-state value of about 550V fast after about 0.35s when active damping is included, while in the absence of active damping, the DC-link voltage attains same steady-state value after about 1.6s. Another benefit of the active damping is that the resulting DC-link voltage signal is smoother without oscillations.

At 50% grid voltage dip, the DC-link voltage experiences exponential rise at zero active damping. This rise may be as a result of decrease in the modulation voltage and hence decrease in the modulation index of the grid-side converter. The DC-link voltage variation during grid voltage dip has almost the same magnitude of variation with active damping and zero active damping but in opposite sense.

Perhaps the benefit of active damping is mostly experienced during grid fault caused by three-phase to ground short-circuit. Against the astronomical DC-link voltage rise of about 1300V from 550V at zero active damping, a DC-link voltage decrease of about 320V is recorded when active damping is introduced. For the zero active damping condition, after the occurrence of the fault the DC-link current increases. Fig. 18 shows DC-link exponential current rise from about 10A peak-to-peak to about 150A peak-to-peak for the 0.5s fault duration. Owing to the grid-side converter voltage drop which is reflected in the d-axis converter voltage $v_d$ as shown in Fig. 25, the GSC can not exchange this extra current to the network according to the power balance of Eqn. (18). This condition leads to the accumulation of charges on the DC-link capacitor and consequently the DC-link voltage rises rapidly according to the DC-link current-voltage relationship: $v_{DC} = C \, di_{DCg}/dt$. At fault, therefore, the power balance of Eqn. (18) no longer holds because even as the d-axis current increases as in Figs. 23 and 24 with active and without active damping respectively, the d-axis voltage decreases.

Fig. 19 shows the variation of the DC-link current for the active damping condition. After the initial transient increase from about 2A as a result of the fault, it starts to decrease from about 30A to about 22A. Instead of the accumulation of charges on the DC-link capacitor the charges are depleted and consequently the DC-link voltage drops rapidly.

A margin is usually set for the DC-link voltage within which the converter sub-system is allowed to still remain in operation without disconnecting it from the grid under faulty condition. DC-link voltage change from 550V to 1300V will for sure excite a protection scheme to disconnect the converter sub-system from the rest of the network, thereby disenabling the converter sub-system ride-through capability.

Application of active damping to the control of GSC provides for the ride-through capability in the event of fault in the network. Instead of rapid increase in the DC-link voltage there will be a reduction in the DC-link voltage to a value which shall depend on the severity, duration, and location of the fault. For the system under study, the DC-link voltage decay is about 42% as against the 136% increase at zero active damping condition.

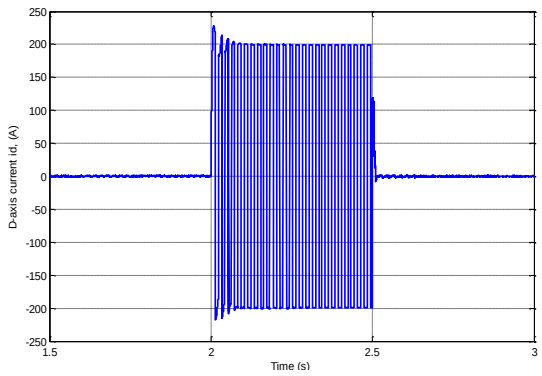


**Fig. 23** D-axis current $i_d$, with active damping.

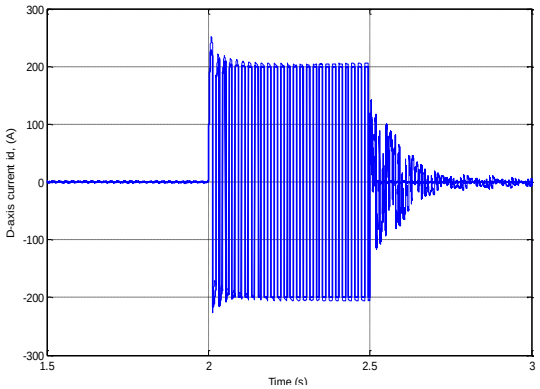


**Fig. 24** D-axis current $i_d$, without active damping.

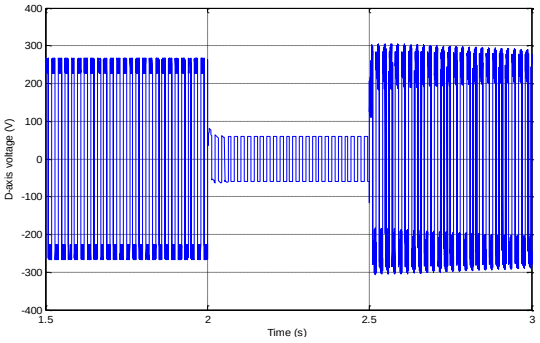


**Fig. 25** D-axis voltage $v_d$.

## 5. CONCLUSIONS

Analysis and verification of the effect of active damping on the dynamic performance of a grid-side converter is presented. When the current control loop is actively damped, it is observed that: a faster dynamic response is achieved for the DC-link voltage as against a sluggish and ripple-infested response when the current control loop is not actively damped. Under fault condition, a 42% decrease in DC-link voltage is realized when active damping is considered. This is against 136% increase in the DC-link voltage when active damping is not considered. The 136% increase in the DC-link voltage may excite the protective breaker to disconnect the grid-side converter (GSC) subsystem from the rest of the network and thus disenable the ride-through capability of the GSC subsystem.

Some schemes may be designed such that the DC-link voltage may operate within a specified range without exciting the protective system or dropping below a set value. A method of maintaining the DC-link voltage within a regulated range forms the topic of next paper.

## 6. REFERENCES

[1] R. Datta, and V. T. Ranganathan, "Decoupled Control of Active and Reactive Power for a Grid-connected Doubly-fed Wound Rotor Induction Machine without Position Sensors," *IEEE Trans. Ind. Applicat*., vol. 4, pp. 2623 – 2630, 3-7 Oct. 1999.

[2] S. K. Salman, and B. Badrzadeh, "New Approach for Modeling Doubly-Fed Induction Generator (DFIG) for grd-connection studies," *www.2004ewec.info/files/23_sksalman_01*.

[3] B. C. Babu K. B. Mohanty, and C. Poongothai, "Wind Turbine Driven Doubly-Fed Induction Generator with Grid Disconnection," *http://eeeic.eu/proc/papers/6.pdf*.

[4] A. D. Hansen, F. lov, P. Sorensen, N. Cutululis, C. Jauch, F. Blaabjerg. "Dynamic wind turbine models in power system simulation tool," *DlgSILENT, Technical University of Denmark Roskilde, Denmark*, August 2007.

[5] M. Molinas, B. Naess, W. Gullvik, and T. Undeland, "Cage Induction Generatorsfor Wind Turbines with Power Electronics Converters in the Light of the New Grid Codes," *http://ieeexplore.ieee.org/xpl/mostRecentIssue.jsp?punumber=11048*

[6] B. Hopfensperger, D. J.Atkinson, and R. A. Lakin "Stator-flux-oriented control of a doubly-fed induction machine with and without osition encoder," *IEEE Proc., Power Appl*., vol. 147, pp. 241 – 250, July 2000.

[7] B. Rabelo, and W. Hofmann, "Optimal Active and Reactive Power Control with the Doubly-Fed Induction Generator in the MW-Class Wind-Turbines," *IEEE Proc., Power Electrons*., vol. 1, pp. 53 – 58, Oct. 2001.

[8] A. Petersson, *Analysis, Modeling and Control of Doubly-Fed Induction Generator for Wind Turbines*, Thesis for the degree of Doctor of Philosophy, Chalmers University of Technology, G'oteborg, Sweden 2005.

[9] R. Ottersten, *On Control of Back-to-Back Converters andSensorless Induction Machine Derives*, PhD-thesis Chalmers University, Gotenborn, Sweden, 2003.

[10] R. Pena, J. C. Clara, and G. M. Asher, "Doubly fed induction generator using back-to-back PWM Converters and its application to variable-speed wind-energy generation," *IEE Proc., Electr. Power Appl*., vol, 143, pp. 231 – 241, May 1996.

[11] J. Morren, *Grid support by power electronic converters of Distributed Generation Units*, Thesis for the degree of Doctor of Philosophy. Delft University of technology (TU-Delft), the Netherlands.

[12] L. Hernefors, and H. P. Nee, "Model-Based Current Control of AC Machines Using the Internal Model Control Method," *IEEE Trans. Ind. Applicat*., vol. 34, pp. 133 – 141, Jan/Feb. 1998.